Liquid Crystals
Publication details, including instructions for authors and subscription information:
http://www.informaworld.com/smpp/title~content=t713926090

Mesomorphism of *ortho*-metallated imine complexes of the β-diketonatoplatinum(II) fragment. Crystal and molecular structure of three platinum imine complexes

Viorel Cîrcu[a]; Peter N. Horton[b]; Michael B. Hursthouse[b]; Duncan W. Bruce[a]
[a] Department of Chemistry, University of York, Heslington, York YO10 5DD, UK [b] EPSRC Crystallographic Service, Department of Chemistry, University of Southampton, Highfield, Southampton SO17 1BJ, UK

To cite this Article Cîrcu, Viorel , Horton, Peter N. , Hursthouse, Michael B. and Bruce, Duncan W.(2007) 'Mesomorphism of *ortho*-metallated imine complexes of the β-diketonatoplatinum(II) fragment. Crystal and molecular structure of three platinum imine complexes', Liquid Crystals, 34: 12, 1463 — 1472
To link to this Article: DOI: 10.1080/02678290701770343
URL: http://dx.doi.org/10.1080/02678290701770343

Liquid Crystals, Vol. 34, No. 12, December 2007, 1463–1472

Mesomorphism of *ortho*-metallated imine complexes of the *β*-diketonatoplatinum(II) fragment. Crystal and molecular structure of three platinum imine complexes

VIOREL CÎRCU†‡, PETER N. HORTON§, MICHAEL B. HURSTHOUSE§ and DUNCAN W. BRUCE*†

†Department of Chemistry, University of York, Heslington, York YO10 5DD, UK

‡Inorganic Chemistry Department, University of Bucharest, 23 Dumbrava Rosie st., 020464, sector 2, Bucharest, Romania

§EPSRC Crystallographic Service, Department of Chemistry, University of Southampton, Highfield, Southampton SO17 1BJ, UK

(*Received 9 August 2007; accepted 23 October 2007*)

The synthesis of a series of *ortho*-metallated Pt imine complexes bound to a range of *β*-diketonato ligands is described and the crystal structures of three are reported; two show unusually short F···F contacts in the solid state. All but one of the new complexes show liquid crystal mesophases and the thermal behaviour was studied using a combination of optical microscopy and differential scanning calorimetry. The mesomorphism is compared with that of analogous palladium complexes reported previously.

1. Introduction

ortho-Metallated complexes represent one of the most interesting and broadly studied classes of metallomesogens (metal complexes with liquid crystal properties), and consist of both dinuclear and mononuclear organometallic systems [1].

These complexes provide a convenient way for the preparation of new systems, the chemical and physical properties of which can be modulated by systematic change of the ligands around the metal centre: heteroaromatic ligands bound in an *ortho*-metallated fashion to one side with different lengths of flexible alkyl or alkoxy chains and various co-ligands on the other side of the metal centre, such as *β*-diketonates, cyclopentadienyl, dialkyldithiocarbamate, etc. Amongst the heteroatomic ligands used in the design of such systems, imine ligands have been employed extensively in cyclometallation reactions and have shown a strong tendency to form, with palladium and platinum precursors, five-membered, cyclometallated rings containing the metal in the +2 oxidation state in a square-planar environment [2].

In our search for suitable candidates for the elusive biaxial nematic phase, we have previously investigated a series of palladium(II) complexes based on *ortho*-metallated imine ligand and various *β*-diketonates [3–5]. The approach used in this work was to design metallomesogens likely to introduce lateral correlations to promote order in directions orthogonal to the main director and hence potentially stabilize a biaxial nematic phase [6, 7]. However, it is important that any such correlations were not too strong in order to prevent the formation of layered (smectic) phases. The principles of this approach, which are also related to computational studies by Berardi and Zannoni [8], are described in more detail in previous publications [3, 6]. It is inappropriate to repeat these details here, but it is enough to say that we wished to exploit the fact that fluorocarbon fragments have a tendency to self-associate and to phase separate from related hydrocarbon moieties, and so introduction of lateral fluorine substituents was a key design goal.

We have now extended this study to related complexes of platinum(II), and several mononuclear species have been synthesized by cleaving chloro-bridged dinuclear complexes with sodium salts of corresponding *β*-diketonates. The new compounds have been characterized chemically by elemental analysis, ^{1}H NMR spectroscopy and, in three cases, single-crystal X-ray diffraction. The complexes described consist of a single imine ligand, whereas the *β*-diketone was varied.

*Corresponding author. Email: db519@york.ac.uk

Liquid Crystals
ISSN 0267-8292 print/ISSN 1366-5855 online © 2007 Taylor & Francis
http://www.tandf.co.uk/journals
DOI: 10.1080/02678290701770343

2. Results and discussion

2.1. *Synthesis*

The synthetic pathways used to prepare the compounds are depicted in scheme 1. The dinuclear chloro-bridged *ortho*-platinated compounds (**1** and **2**) were obtained by *ortho*-platination of the imines [9] bases using [Pt(μ-Cl)(η^3-C_4H_7)]$_2$ as starting material [10].

The preparation of mononuclear *ortho*-platinated complexes **3e**–**3f**, **4a**–**4g** was carried out by ligand exchange reaction of the chloro-bridged dinuclear platinum complexes (**1** and **2**) using the sodium salts of the corresponding acetylacetone. The new, mononuclear complexes were obtained in moderate-to-good yields as red, microcrystalline solids. When the β-diketone derivative is unsymmetric, the final products (**4c**–**4f**) contain a mixture of the two possible *syn* and *anti* isomers. The proportion of these two isomers in the final mixture was evaluated from the ^{1}H NMR spectroscopy by integrating the corresponding signals. Indeed, the formation of these *ortho*-platinated species can be confirmed readily by ^{1}H NMR spectroscopy (figure 1) where a pattern specific to a 1,3,4-substitution of an aromatic ring can be seen as two doublets and a doublet of doublets. Also, the signal corresponding to the imine proton appears in the region δ 8–9 due to a deshielding effect, whereas the singlet in the region δ 5–6 was assigned easily to the methyne proton from the β-diketone derivative. Another interesting feature of the ^{1}H NMR spectra is the presence of the ^{195}Pt satellites which, once again, confirm the *ortho*-platination process and from which the coupling constants $^3J_{Pt-H}$ were deduced. The values were in the expected range for such compounds and similar with those found for other *ortho*-platinated compounds [11].

2.2. *Single-crystal X-ray structures*

Single crystals of compounds **3e**, **3f** and **4e** suitable for analysis by single-crystal X-ray diffraction were obtained from a mixture of acetone and methanol (ca. 1/1 v/v) at -25°C (note that only a very few crystals of **3f** were available and so there is no other characterization

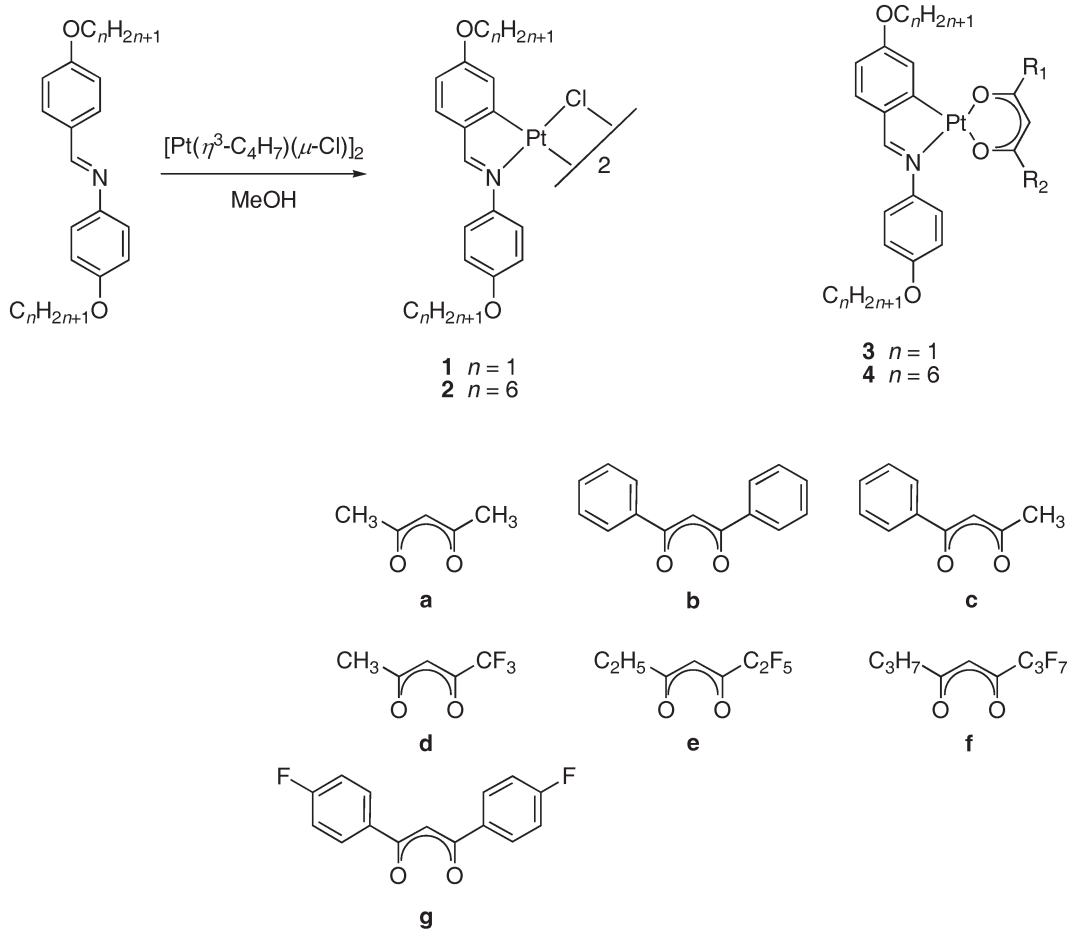

Scheme 1. Synthesis of the new complexes and the β-diketonates used

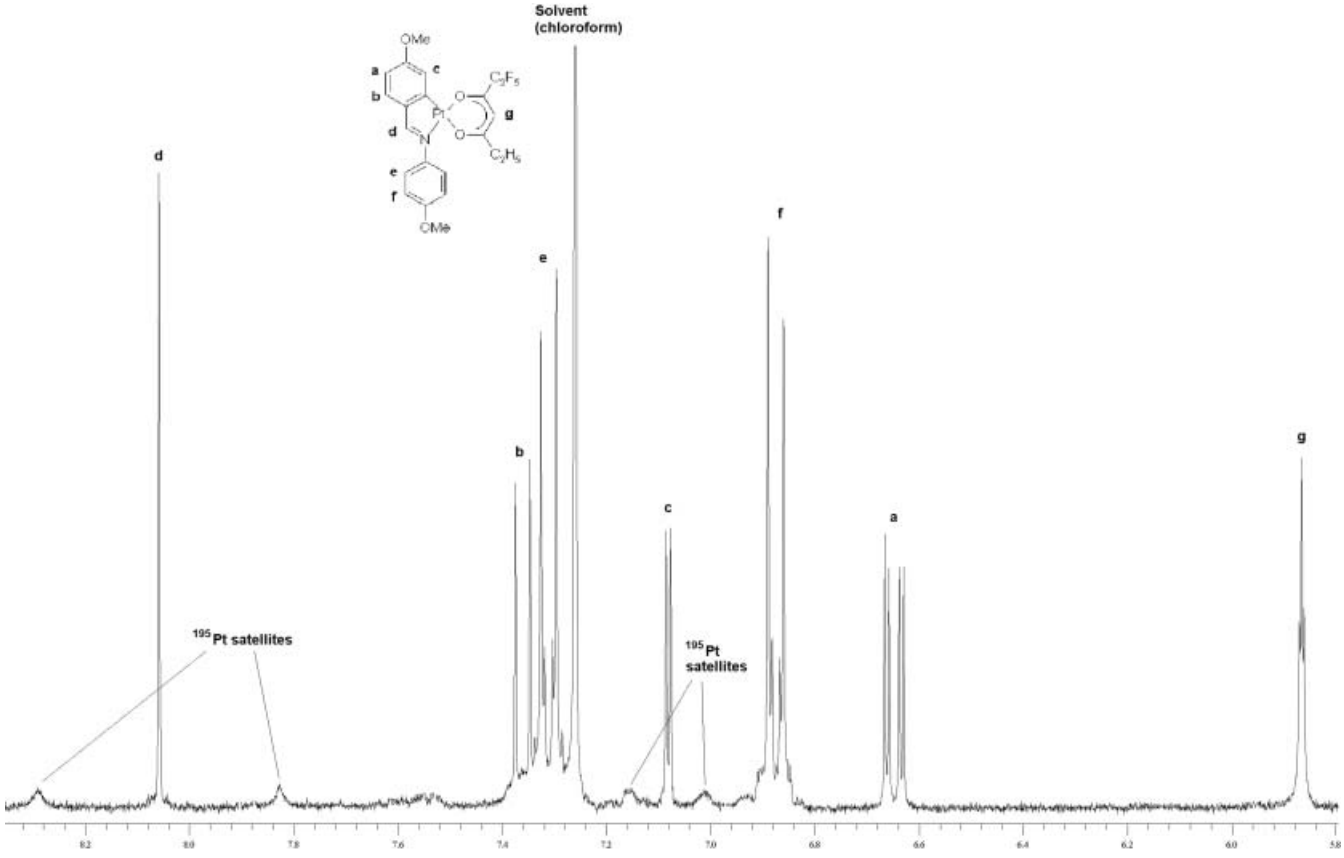

Figure 1. The aromatic region of the ^{1}H NMR spectrum of compound **3e** showing the coupling to ^{195}Pt.

of this complex). Complexes **3e** and **4e** both crystallized as dimers with two, independent molecules in the structural unit. Crystallographic information is collected in table 1, whereas selected bond lengths and angles for all three complexes are presented in table 2.[†]

The molecular structure of **3e** is shown in figure 2. Complex **3e** crystallized in monoclinic crystal system, space group $P2_1/n$, with the platinum atom surrounded by two oxygen atoms of the two carbonyl groups, one aromatic carbon atom (metallated phenyl ring) and one nitrogen atom (imine group) in a square-planar arrangement with *syn* configuration (the perfluoroethyl group is *cis* to the nitrogen atom of the imine group. The corresponding chelate rings around the Pt centre are essentially planar with a maximum deviation from the mean plane of 0.029 Å and 0.037 Å for Pt_1 and Pt_2, respectively.

From figure 2 it can be seen that the structure of **3e** is arranged in the less common *syn* configuration (perfluoroethyl group is *cis* to nitrogen atom of the imine group), similar to its palladium analogue [4]. The Pt–Pt distance between the two independent molecules is 7.46 Å, precluding Pt–Pt interactions. Whereas the metallated phenyl ring is almost coplanar with respect to the mean plane, the unmetallated ring of the imine ligand is twisted by 47.7° for one molecule, and by 51.4° for the second molecule with respect to the core plane. In addition, there is a significant proximity between the fluorine atom attached to the carbon atom in α position (with respect to the carbonyl group) and the terminal CF_3 group of the neighbouring molecule (see figure 3). The distance between the two corresponding fluorine atoms is 2.73 Å, which puts them within the range of non-bonded interaction (the van der Waals radius of fluorine is 1.47 Å) [12]. Although the nature of F···F interactions is controversial and their presence is rare and generally considered as being weak [13], the interaction present in the case of **3e** can be explained by the strong electron-withdrawing character of the carbonyl group, which makes the fluorine atoms in the α position more positive than the terminal ones, thus giving rise to a dipolar interaction. Another factor that contributes to the crystal packing of **3e** are intermole-

[†] CCDC-652747, CCDC-652748 and CCDC-652749 contain the supplementary crystallographic data for this paper. These data can be obtained free of charge from The Cambridge Crystallographic Data Centre *via* www.ccdc.cam.ac.uk/data_request/cif.

Table 1. Crystallographic data for **3e**, **3f** and **4e**.

	3e	**3f**	**4e**
Empirical formula	$C_{22}H_{20}F_5NO_4Pt$	$C_{24}H_{22}F_7NO_4Pt$	$C_{32}H_{40}F_5NO_4Pt$
Formula weight/g mol^{-1}	652.48	716.52	792.74
T/K	120(2)	120(2)	120(2)
λ/Å	0.71073	0.71073	0.71073
Crystal system	monoclinic	monoclinic	monoclinic
Space group	$P2_1/n$	$P2_1/c$	$P2_1/c$
Unit cell dimensions/Å	a=14.5057(3)	a=14.8790(2)	a=18.6505(3)
	b=11.5897(3)	b=12.0240(2)	b=10.5350(2)
	c=26.1769(6)	c=14.6050(2)	c=33.7505(7)
Unit cell angles/°	α=90	α=90	α=90
	β=102.3040(10)	β=111.4000(7)	β=96.9940(10)
	γ=90	γ=90	γ=90
Volume/Å^3	4299.69(17)	2432.76(6)	6582.1(2)
Z	8	4	8
ρ_{calc}/Mg m^{-3}	2.016	1.956	1.600
Absorption coefficient/mm^{-1}	6.600	5.853	4.327
F(000)	2512	1384	3152
Crystal	Cone; Red	Slab; Orange	Blade; Orange
Crystal size/mm^3	0.60 × 0.25 × 0.10	0.13 × 0.09 × 0.03	0.16 × 0.08 × 0.03
θ range for data collection	2.94–27.48°	2.98–27.48°	2.93–27.48°
Index ranges	$-18 \leqslant h \leqslant 18$, $-15 \leqslant k \leqslant 14$, $-33 \leqslant l \leqslant 33$	$-19 \leqslant h \leqslant 19$, $-15 \leqslant k \leqslant 15$, $-18 \leqslant l \leqslant 18$	$-24 \leqslant h \leqslant 24$, $-13 \leqslant k \leqslant 13$, $-43 \leqslant l \leqslant 43$
Reflections collected	49368	28836	57990
Independent reflections	9807 [R_{int}=0.0798]	5563 [R_{int}=0.0306]	14999 [R_{int}=0.1225]
Completeness to θ=27.48°	99.6%	99.6%	99.3%
Absorption correction	Semi−empirical from equivalents	Semi−empirical from equivalents	Semi−empirical from equivalents
Max. and min. transmission	0.5582 and 0.1097	0.8440 and 0.5166	0.8812 and 0.5444
Refinement method	Full-matrix least-squares on F^2	Full-matrix least-squares on F^2	Full-matrix least-squares on F^2
Data/restraints/parameters	9807/0/601	5563/0/337	14999/401/807
Goodness-of-fit on F^2	1.119	1.043	1.059
Final R indices [$F^2>2\sigma(F^2)$]	*R1*=0.0356, *wR2*=0.0716	*R1*=0.0186, *wR2*=0.0376	*R1*=0.0887, *wR2*=0.1487
R indices (all data)	*R1*=0.0504, *wR2*=0.0762	*R1*=0.0218, *wR2*=0.0391	*R1*=0.1311, *wR2*=0.1577
Largest diff. peak and hole/e Å^{-3}	2.257 and −1.646	0.581 and −0.719	1.969 and −1.946

Table 2. Selected bond lengths and angles for compounds **3e**, **3f** and **4e**.

	3e		**3f**	**4e**	
Bonds lengths/Å	**Molecule A**	**Molecule B**		**Molecule A**	**Molecule B**
Pt–O	1.987(4)	1.996(4)	1.9984(16)	1.992(7)	2.004(6)
Pt–O	2.084(3)	2.077(3)	2.0876(17)	2.101(6)	2.080(6)
Pt–N	2.000(5)	1.999(4)	2.0020(19)	1.986(8)	2.008(7)
Pt–C	1.968(5)	1.958(5)	1.961(2)	1.983(10)	1.976(11)
C–N (imine)	1.304(7)	1.304(6)	1.302(3)	1.308(12)	1.329(12)
C–O (carbonyl)	1.260(7)	1.267(6)	1.272(3)	1.319(11)	1.302(11)
C–O (carbonyl)	1.282(6)	1.259(6)	1.275(3)	1.262(11)	1.265(11)
Bonds angles/°					
C–Pt–O	91.24(18)	91.72(19)	91.21(8)	93.4(3)	92.0(3)
C–Pt–N	81.3(2)	81.1(2)	81.20(9)	81.4(4)	81.5(4)
O–Pt–O	91.37(14)	91.64(14)	91.16(6)	91.1(3)	91.0(3)
N–Pt–O	96.13(16)	95.46(16)	96.39(7)	94.2(3)	95.4(3)

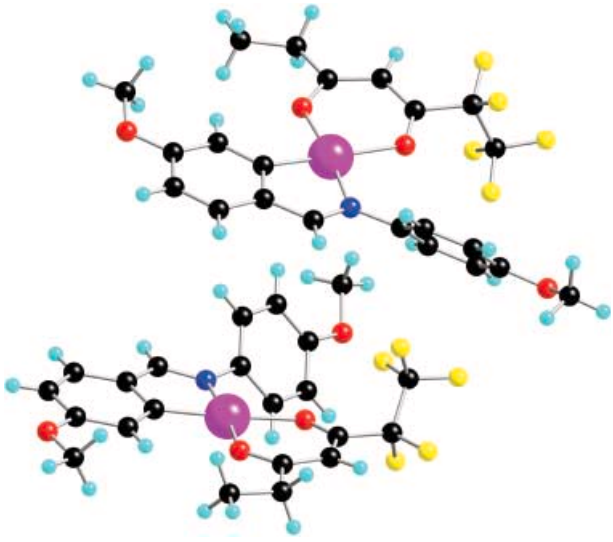

Figure 2. Molecular structure of **3e** showing the two different molecules in the unit cell.

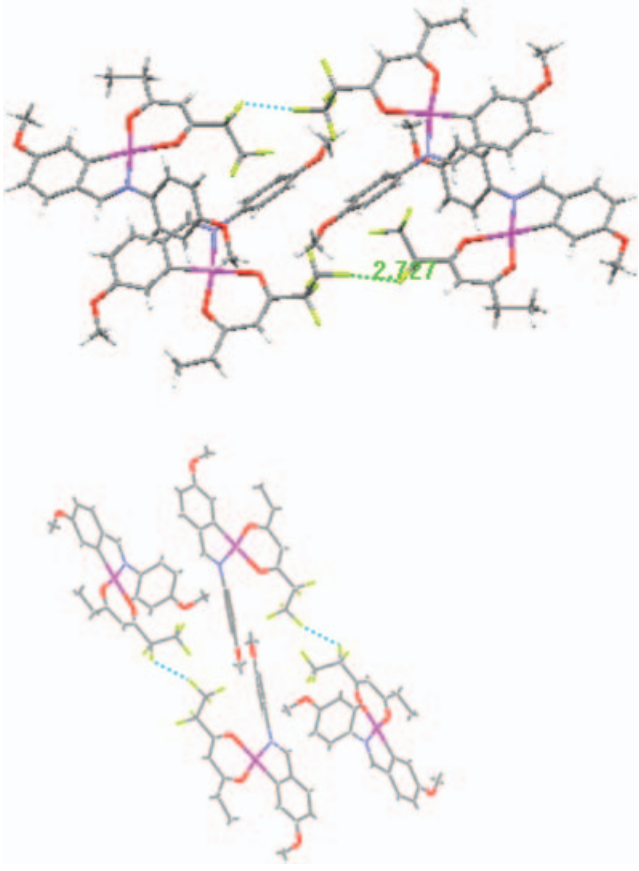

Figure 3. Two views of complex **3e** showing the proximity of the fluorine atoms of neighbouring molecules.

cular –C–H···F–C– interactions, found in the case of terminal CF_3 group and the hydrogen atom in the *para* position in respect with the metallated carbon atom, and between fluorine atoms in α position (with respect to the carbonyl group) and the methoxy group of the aniline ring. In the former case, the measured H···F distance is 2.52 Å, while in the later case it is 2.65 Å. Both values are smaller than the sum of the van der Waals radii of fluorine and hydrogen at 2.67 Å.

Complex **4e** (figure 4) crystallizes in the monoclinic crystal system, group $P2_1/c$, with the same square-planar arrangement around the platinum atom; indeed bond lengths and angles for the central core are all very similar to those found in complex **3e**.The Pt–C distance is similar to those found in dinuclear chloro- or thiocyanato-bridged, *ortho*-metallated platinum compounds with Schiff bases reported by Praefcke *et al.* [14], whereas the Pt–N distances are slightly smaller (2.19 and 2.064 Å in Praefcke's work), which could be assigned to the difference in *trans*-effect of the atoms coordinated to platinum. The same orientation with respect to the core plane was found for the unmetallated ring of the imine ligand, which is twisted by 47.5° for one molecule, and by 47.7° for the second molecule. In this case, the maximum deviations from the mean plane are 0.044 Å and 0.049 Å for Pt_1 and Pt_2, respectively and the Pt–Pt distance between two adjacent molecules is 6.94 Å.

What is very different for this complex with respect to **3e** is the *anti* configuration (the perfluoroethyl group is trans to nitrogen atom of the imine group) adopted by the two ligands around platinum centre. The ^{1}H NMR spectrum of the product isolated from the cleavage reaction of the dinuclear platinum(II) compound indicates a mixture of the two isomers for **4e**, the proportion of the *anti*-isomer being ~70%. Also, the ^{1}H NMR spectrum of a single crystal of **4e** shows only one isomer present in solution, indicating that the isolation of the *anti* isomer is not due to isomerization in solution

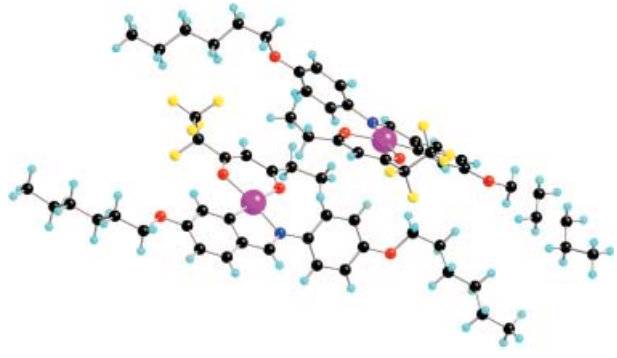

Figure 4. Molecular structure of **4e** showing both molecules in the unit cell.

but the fact that this isomer is less soluble and crystallizes preferentially.

Complex **3f** crystallizes in monoclinic crystal system, group $P2_1/c$, with four discrete molecules in the unit cell (figure 5). The crystal structure of this compound shows Pt(II) in a square planar environment (C(1)–Pt– O(22) 91.21°, C(1)–Pt–N(1) 81.20°, O(21)–Pt–O(22) 91.16, N(1)–Pt–O(21) 96.39°) bound to imine ligand in an *ortho*-metallated fashion and chelated to acetylacetonate derivative with the same coordinated atoms (one aromatic C atom (metallated ring), one N atom (imine group) and two O atoms of the two carbonyl groups) as found for compounds **3e** and **4e**. The two five- and six-membered chelate rings are almost coplanar with the metallated ring of the imine ligand while the unmetallated ring is twisted in respect to the core plane with 50.79°; this value is similar to that found for the other complexes. For this compound the maximum deviation from the mean plane is 0.027 Å and the Pt–Pt distance between two adjacent molecules is 7.525 Å. The same, less common *syn* arrangement as for compound **3e** can be seen for the ligands around Pt(II) metal (in this case the perfluoropropyl group is *cis* to the nitrogen atom of the imine group).

Compared to **3e**, the crystal packing of **3f** (figure 6) shows no obvious F···F interactions yet there are –C–H···F–C– interactions, which were found between the terminal $–CH_3$ group and the fluorine atoms in the β-position with respect to the carbonyl group of the acac derivative. The measured distance is 2.54 Å, which is smaller than the sum of the van der Waals radii of fluorine and hydrogen (2.67 Å).

2.3. *Thermal behaviour*

The mesomorphic properties of the new platinum complexes were studied by polarized optical microscopy and DSC; transition temperatures, enthalpies and

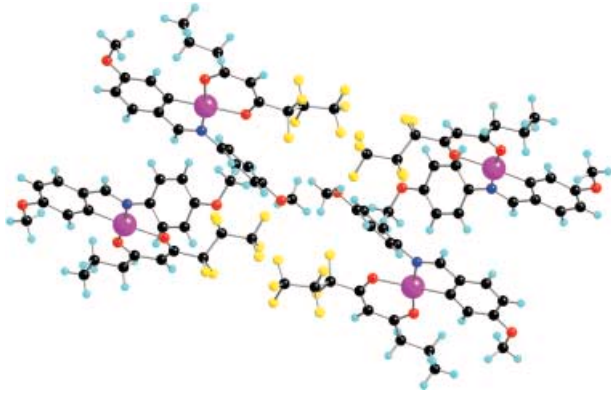

Figure 5. The molecular structure of compound **3f**, showing the four complexes of the unit cell.

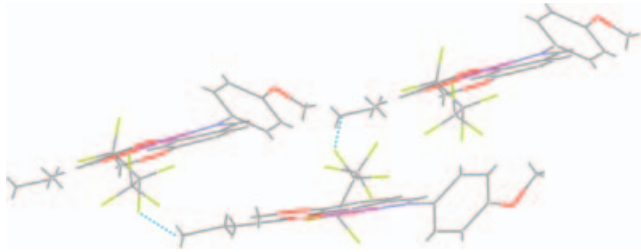

Figure 6. The crysal-packing diagram showing –C–H…F–C– intermolecular interactions.

mesophases observed are collected in table 3. All complexes showed a nematic phase, except compound **3e**, which melted straight to the isotropic phase at 161°C and showed no mesomorphic behaviour, and compound **4g**, which began to decompose when it melted from the solid state into a smectic A (SmA) phase at 144°C.

Replacing one $–CH_3$ group with $–CF_3$ group (**4a** versus **4d**) in the simple acetylacetone co-ligand produces, as expected from our previous studies on analogous palladium compound [3, 5] a noticeable lowering of the clearing point together with a change in the mesomorphic behaviour. Thus, the SmA phase is suppressed when tfac is used and **4d** shows only a monotropic nematic phase, while **4a** shows both enantiotropic SmA and nematic phases.

All three platinum complexes bearing perfluoroalkyl groups (**4d**–**4f**) show the same mesomorphic behaviour with a monotropic nematic phase, which is highly destabilized with the introduction of additional $–CH_2–$/$–CF_2$ groups on β-diketone ligand. Thus, the transition

Table 3. Thermal data for the platinum(II) complexes.

Compound	Transition[a]	T/°C	ΔH/kJ mol^{-1}	ΔS/R
4a	Cr–SmA	79	34.4	12
	SmA–N	143	0.8	0.2
	N–I	149	1.0	0.3
4b	Cr–I	135	42.0	12
	(N–I)	(110)	(0.2)	(0.1)
4c	Cr–SmA	113	21.1	7
	SmA–N	137	0.6	0.2
	N–I	146	0.6	0.2
4d	Cr–I	86	19.1	6
	(N–I)	(75)	(0.7)	(0.2)
4e	Cr–I	94	44.4	15
	(N–I)	(37)	(0.5)	(0.2)
4f	Cr–I	69	36.6	13
	(N–I)	(17)	(0.3)	(0.1)
4g	Cr–SmA (dec)	144	37.5	11

[a] $T_{(N–I)}$ is quoted as we have cooled from isotropic to nematic and then re-heated back to the isotropic. It is the latter temperature that is quoted, representing the true, thermodynamic temperature for the transition.

temperature from the isotropic to nematic phase of compound **4e** is significantly lower (by 38°C) than the corresponding transition temperature of compound **4d** and higher (by 20°C) when compared to the value of **4f**. The same trend was observed for the calculated entropies corresponding to the nematic-to-isotropic transitions deduced from DSC, the smallest being 0.1 ($=\Delta S/R$) for compound **4f**. The melting points of the three platinum complexes do not, however, follow the same trend. Thus, the highest melting point is 94°C for compound **4e**, behaviour which could be explained by the different proportion of the two possible isomers in the mixture.

A strong decrease in clearing temperature, accompanied by a decrease in mesophase range, on increasing the perfluoroalkyl chains length was also observed for the palladium analogues. This effect is, however, different from that found in other fluoroalkylated organometallic mesogens based on dinuclear chloro-bridged palladium complexes in which the fluorine atoms were introduced in the side chains of the imine ligand and led to more stable mesophases with increasing clearing temperature [15].

Indeed, comparison of the mesomorphism of the present complexes with their Pd analogues shows fairly close correspondence in mesomorphism and transition temperatures, and figure 7 shows a comparison of T_{N-I} for complexes of the two metals. It is interesting to note that, in each case, the Pd complex has the lower clearing temperature. In complexes **4c** to **4f** it could be argued that a different proportion of the two possible geometric answers could be the cause, and the relatively small difference observed in the case of **4b** would seem to lend to support this idea. However, the substantial difference in the case of **4a** is not consistent with such a proposition.

The transition temperatures for isomerically pure palladium and platinum complexes which present the same structure, previously reported by Buey *et al.* [9, 16], are higher for the platinum complexes and is a consequence of replacing palladium with the heavier platinum metal which brings an enhancement in polarizability.

The other important point of comparison relates to the thermodynamics of the N-to-I transition. The original theoretical work on the biaxial nematic phase suggests that direct I-to-N_B transition ought to occur at a Landau point, where the transition would be second order and so the entropy (and enthalpy) change would be zero. Initial work with the Pd analogue of **4d** revealed a rather small entropy of transition (and, interestingly, a small transitional order parameter), but the observation of coexisting isotropic and nematic phases by ^{2}H NMR spectroscopy showed the transition to be first order. The extended studies of *β*-diketonatopalladium(II) complexes revealed a number of complexes with small entropies of transition, which require further study. However, it also showed that relatively small increases in lateral dipole (*via* the *β*-diketonate) induced smectic behaviour. Interestingly, the Pt complexes reported here show entropies of transition that are the same as, or remarkably close

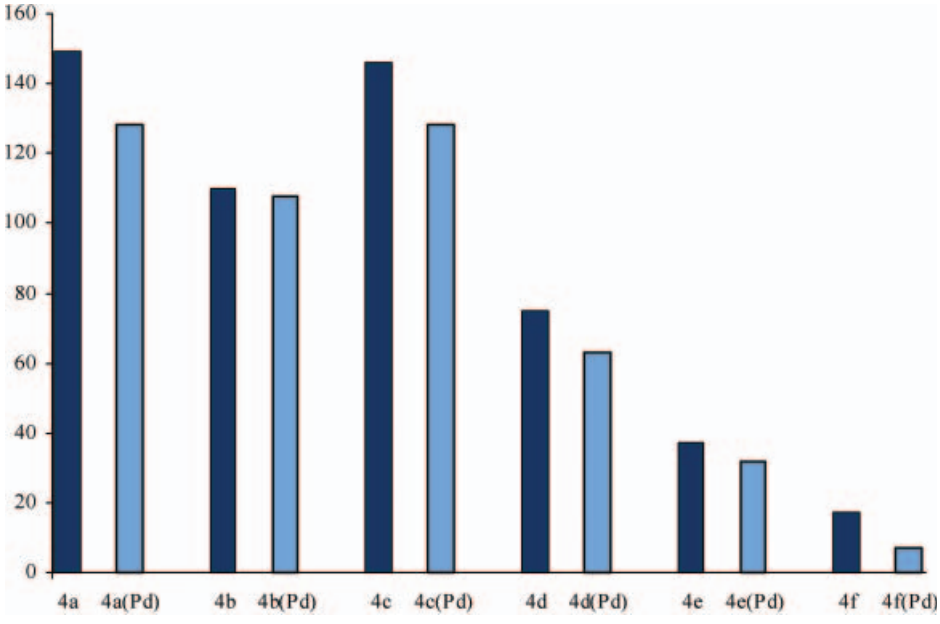

Figure 7. Comparison of T_{N-I} (in °C) for the new complexes alongside their Pd analogues.

to, those of their Pd congeners. However, what this does suggest is that given the increased complexity of the synthesis of the Pt complexes (involving the pre-preparation of di-μ-(chloro)bis(η^3-2-methallyl)-diplatinum(II) and the lower yields for the preparation of the dinuclear precursor complex), the palladium complexes represent preferable targets for further, detailed study.

Finally, one, additional point is worth making. The theories surrounding I-to-N_B transitions have for a long time suggested that this transition ought to be second order at a Landau point. However, recent work by Bisi *et al.* [17] has suggested that the transition could in fact be first order and that it can be found for a range of molecular forms along a Landau *line*.

Similarly, whereas computational studies of jointed, bent-core mesogens showed a Landau point for the I-to-N_B transition at a critical angle 109°28′ [18], Bates has used a lattice model to show that either by increasing the flexibility of the system [19] or by introducing a lateral dipole [20], the Landau point splits to form a Landau line where first-order I-to-N_B transitions can be observed. Thus, adding a little chemical 'reality' to the computational model suggests a more flexible approach to the chemical design. Greater 'chemical reality' has not, to date, been applied to the original models from which predictions of the N_B phase arose, but it is not impossible to imagine that the form of the phase diagram could change to offer the synthetic chemist a better chance of successful molecular design. Thus, in these β-diketonato complexes, the order of the I-to-N transition may not be the critical matter that had been supposed. Thus, the development of liquid crystal design by the close interplay of theory, simulation and design will continue to represent an optimal way forward.

3. Experimental

Dichloromethane was distilled from phosphorus pentoxide; other chemicals were used as supplied. ^{1}H NMR spectra were recorded on a Bruker DFX 400 MHz spectrometer using $CDCl_3$ as solvent. ^{1}H chemical shifts were referenced to the solvent peak position, δ 7.26.

Elemental analyses were performed in the Department of Chemistry, University of Exeter. Analysis by DSC was carried out using a Perkin-Elmer DSC7 instrument using various heating rates. Mesomorphism was studied by hot stage polarizing microscopy using a Zeiss Labpol microscope equipped with a Linkam TH600 hot stage and PR600 temperature controller. Mesophases were assigned by their optical textures.

Suitable single crystals were selected and data collected on a Bruker Nonius KappaCCD Area Detector at the window of a Bruker Nonius FR591 rotating anode ($\lambda_{Mo\text{-}K\alpha}$=0.71073 Å) driven by COLLECT [21] and DENZO [22] software at 120 K. Structures were determined in SHELXS-97 [23] and refined using SHELXL-97 [18]. All hydrogen atoms were fixed.

All the chemicals used in this work for preparation of β-diketonate derivatives and imine ligands and were commercially available from Lancaster. The β-diketonate ligands were bought from Lancaster or prepared using the methods published in literature [24]. The starting platinum material di-μ-(chloro)bis(η^3-2-methallyl)-diplatinum(II) was prepared from $K_2[PtCl_4]$ and 3-chloro-2-methyl-1-propene, as described elsewhere [10]. The imine ligands were prepared by acetic acid catalysed condensation of the corresponding aldehyde and amine in absolute ethanol while the dinuclear platinum(II) complexes were prepared by an *ortho*-platination reaction between di-μ-(chloro)bis(η^3-2-methallyl)diplatinum(II) and the imine ligands in methanol using the procedure described by Buey *et al.* [9].

3.1. *Preparation of mononuclear platinum(II) complexes*

One equivalent of dinuclear compound was reacted with two equivalents of sodium salts of acetylacetone derivatives in dichloromethane, at room temperature with stirring for 24 h. The solvent was removed and the residue was purified on silica using dichloromethane as eluant. Crystallization from acetone/methanol 1:1 gave the mononuclear compounds as red crystalline solids.

Preparation of compound **4a** was described by Buey *et al.* [9]. This compound was synthesized for comparison purposes. Single crystals of **3e**, **3f** and **4e** were grown from acetone/methanol mixture at −25°C.

For **3e**, yield 33%. Elemental analysis: calculated for $C_{22}H_{21}F_5NO_4Pt$, C 40.5, H 3.1, N 2.2; found, C 40.6, H 3.2, N 2.0%. ^{1}H NMR (δ, 300 MHz, $CDCl_3$): 8.06 (1H, s, $^3J_{Pt-H}$=138.1 Hz), 7.36 (1H, d, $^3J_{HH}$=8.5 Hz), 7.31 (2H, d, AA′XX′, $^3J_{HH}$=9.1 Hz), 7.08 (1H, d, $^4J_{HH}$=2.5 Hz, $^3J_{Pt-H}$=44.3 Hz), 6.87 (2H, d, AA′XX′, $^3J_{HH}$=8.9 Hz), 6.65 (1H, dd, $^3J_{HH}$=8.5 Hz, $^4J_{HH}$=2.5 Hz), 5.87 (1H, t, broad), 3.90 (3H, s), 3.84 (3H, s), 2.33 (2H, q, $^3J_{HH}$=7.5 Hz), 1.29 (3H, t, $^3J_{HH}$=7.5 Hz). Only one isomer is present in solution, the *syn* isomer as confirmed by X-ray diffraction. M.p. 161°C.

For **4a**, yield 27%. Elemental analysis: calculated for $C_{30}H_{42}NO_4Pt$, C 53.4, H 6.1, N 2.1; found, C 53.1, H 6.3, N 1.9%. ^{1}H NMR (δ, 300 MHz, $CDCl_3$): 8.11 (1H, s, $^3J_{Pt-H}$=131 Hz), 7.36 (2H, d, AA′XX′, $^3J_{HH}$=9.1 Hz), 7.32 (1H, d, $^3J_{HH}$=8.4 Hz), 7.11 (1H,

d, $^4J_{HH}$=2.4 Hz, $^3J_{Pt-H}$=42.8 Hz), 6.88 (2H, d, AA′XX′, $^3J_{HH}$=9.1 Hz), 6.59 (1H, dd, $^3J_{HH}$=8.4 Hz, $^4J_{HH}$=2.4 Hz), 5.39 (1H, s), 4.07 (2H, t, $^3J_{HH}$=6.6 Hz), 3.97 (2H, t, $^3J_{HH}$=6.6 Hz), 1.97 (3H, s), 1.85–1.32 (19H, m), 0.94–0.88 (6H, m).

For **4b**, yield 50%. Elemental analysis: calculated for $C_{40}H_{46}NO_4Pt$, C 60.1, H 5.6, N 1.7; found, C 59.7, H 5.5, N 1.8%. ^{1}H NMR (δ, 300 MHz, $CDCl_3$): 8.18 (1H, s, $^3J_{Pt-H}$=132 Hz), 8.05 (2H, d, $^3J_{HH}$=8.5 Hz), 7.77 (2H, d, AA′XX′, $^3J_{HH}$=8.5 Hz), 7.54–7.26 (10H, m), 6.95 (2H, d, AA′XX′, $^3J_{HH}$=8.9 Hz), 6.77 (1H, s), 6.63 (1H, dd, $^3J_{HH}$=8.3 Hz, $^4J_{HH}$=2.4 Hz), 4.13 (2H, t, $^3J_{HH}$=6.8 Hz), 4.02 (2H, t, $^3J_{HH}$=6.5 Hz), 1.86–1.33 (16H, m), 0.94–0.88 (6H, m).

For **4c**, yield 62%. Elemental analysis: calculated for $C_{35}H_{44}NO_4Pt$, C 57.1, H 5.9, N 1.9; found, C 57.0, H 5.8, N 2.0%. ^{1}H NMR (δ, 300 MHz, $CDCl_3$): 8.14 (syn), 8.13 (anti) (1H, s, $^3J_{Pt-H}$=131 Hz), 7.97 (syn), 7.66 (anti) (2H, d, AA′XX′, $^3J_{HH}$=7.9 Hz), 7.46–7.37 (4H, m), 7.35 (1H, d, $^3J_{HH}$=8.5 Hz), 7.29 (1H, d, $^3J_{HH}$=7.9 Hz), 7.15 (1H, d, $^4J_{HH}$=2.4 Hz, $^3J_{Pt-H}$=41 Hz), 6.93 (2H, d, AA′XX′, $^3J_{HH}$=8.9 Hz), 6.61 (1H, dd, $^3J_{HH}$=8.5 Hz, $^4J_{HH}$=2.4 Hz), 6.11 (anti), 6.05 (syn) (1H, s), 4.10 (2H, t, $^3J_{HH}$=6.5 Hz), 4.00 (2H, t, $^3J_{HH}$=6.5 Hz), 2.16 (syn), 2.10 (anti) (3H, s), 1.85–1.32 (16H, m), 0.94–0.88 (6H, m). Isomer ratio: 17:83.

For **4d**, yield 60%. Elemental analysis: calculated for $C_{30}H_{39}F_3NO_4Pt$, C 49.5, H 5.3, N 1.9; found, C 49.4, H 5.1, N 1.6%. ^{1}H NMR (δ, 300 MHz, $CDCl_3$): 8.05 (syn), 8.04 (anti) (1H, s, $^3J_{Pt-H}$=138.1 Hz), 7.36–7.30 (3H, m), 7.00 (1H, d, $^4J_{HH}$=2.3 Hz, $^3J_{Pt-H}$=39.2 Hz), 6.91–6.85 (2H, m), 6.64–6.59 (1H, m), 5.83 (syn), 5.80 (anti) (1H, s), 4.07 (2H, t, $^3J_{HH}$=6.8 Hz), 3.98 (2H, m), 2.07 (syn), 1.87 (anti) (3H, s), 1.85–1.34 (16H, m), 0.95–0.89 (6H, m). Isomer ratio: 50:50.

For **4e**, yield 54%. Elemental analysis: calculated for $C_{32}H_{41}F_5NO_4Pt$, C 48.5, H 5.0, N 1.8; found, C 48.0, H 5.0, N 1.8%. ^{1}H NMR (δ, 300 MHz, $CDCl_3$): 8.05 (syn), 8.02 (anti) (1H, s, $^3J_{Pt-H}$=138 Hz), 7.34–7.26 (3H, m), 7.04 (anti), 6.98 (syn) (1H, d, $^3J_{Pt-H}$=43 Hz, $^4J_{HH}$=2.4 Hz), 6.84 (anti) (2H, d, AA′XX′, $^3J_{HH}$=8.8 Hz), 6.62 (anti) (1H, dd, $^3J_{HH}$=8.3 Hz, $^4J_{HH}$=2.3 Hz), 5.89 (syn), 5.85 (anti) (1H, s), 4.06 (2H, t, $^3J_{HH}$=6.6 Hz), 3.96 (2H, t, $^3J_{HH}$=6.6 Hz), 2.32 (anti), 2.16 (syn) (2H, q, $^3J_{HH}$=7.5 Hz), 1.85–0.90 (25H, m). Isomer ratio: 29:71.

For, **4f**, yield 67%. Elemental analysis: calculated for $C_{34}H_{43}F_7NO_4Pt$, C 47.6, H 5.1, N 1.6; found, C 47.1, H 5.2, N 1.9%. ^{1}H NMR (δ, 300 MHz, $CDCl_3$): 8.03 (syn), 8.02 (anti) (1H, s), 7.33–7.26 (3H, m), 7.01 (anti), 6.96 (syn) (1H, d, $^4J_{HH}$=2.4 Hz,), 6.87 (syn), 6.83 (anti) (2H, d, AA′XX′, $^3J_{HH}$=8.9 Hz), 6.61 (anti) (1H, dd, $^3J_{HH}$=8.3 Hz, $^4J_{HH}$=2.4Hz), 5.85 (syn), 5.80 (anti) (1H, s), 4.05 (2H, t, $^3J_{HH}$=6.7 Hz), 3.94 (2H, t, $^3J_{HH}$=6.6 Hz), 2.25 (anti), 2.05 (syn) (2H, t, $^3J_{HH}$=7.4 Hz), 1.80–1.31 (18H, m), 0.92 (anti) (3H, t, $^3J_{HH}$=7.3 Hz), 0.89 (6H, m), 0.80 (syn, 3H, t). Isomer ratio: 33:67.

For **4g**, yield 65%. Elemental analysis: calculated for $C_{40}H_{44}F_2NO_4Pt$, C 57.5, H 5.2, N 1.7; found, C 57.6, H 5.1, N 1.5. ^{1}H NMR (δ, 300 MHz, $CDCl_3$): 8.17 (1H, s, $^3J_{Pt-H}$=133 Hz), 8.05 (2H, AA′MXX′, $^3J_{HH}$=8.9 Hz, $^4J_{HF}$=5.5 Hz), 7.74 (2H, AA′MXX′, $^3J_{HH}$=8.9 Hz, $^4J_{HF}$=5.5 Hz), 7.44 (2H, AA′XX′, $^3J_{HH}$=8.9 Hz), 7.31 (1H, d, $^3J_{HH}$=8.3 Hz), 7.23 (1H, d, $^4J_{HH}$=2.5 Hz), 7.12 (2H, AA′MXX′, $^3J_{HH}$=8.7 Hz), 7.02–6.93 (4H, m), 6.67–6.63 (2H, m), 4.12 (2H, t, $^3J_{HH}$=6.8 Hz), 4.02 (2H, t, $^3J_{HH}$=6.6 Hz), 1.90–1.33 (16H, m), 0.97–0.89 (6H, m).

Acknowledgements

We thank NATO and MEdC (Romanian Ministry of Education) for funding (VC), and Johnson Matthey for generous loans of $K_2[PtCl_4]$.

References

[1] For a review of *ortho*-palladated systems, see B. Donnio, D.W. Bruce. In *Palladacycles*, J. Dupont, M. Pfeffer (Eds), Wiley-VCH, Weinheim (2008).
[2] B. Donnio, D. Guillon, R. Deschenaux, D.W. Bruce. In *Comprehensive Coordination Chemistry II*, J.A. McCleverty, T.J. Meyer (Eds). Vol. 7, Chap. 7.9, pp. pp. 357–627, Elsevier, Oxford (2003).
[3] V. Cîrcu, T.J.K. Gibbs, L. Omnès, P.N. Horton, M.B. Hursthouse, D.W. Bruce. *J. Mater. Chem.*, **16**, 4316 (2006).
[4] L. Omnès, V. Cîrcu, P.T. Hutchins, S.J. Coles, P.N. Horton, M.B. Hursthouse, D.W. Bruce. *Liq. Cryst.*, **32**, 1437 (2005).
[5] L. Omnès, B.A. Timimi, T. Gelbrich, M.B. Hursthouse, G.R. Luckhurst, D.W. Bruce. *Chem. Commun.*, 2248 (2001).
[6] D.W. Bruce. *Chem. Rec.*, **4**, 10 (2004).
[7] G.R. Luckhurst. *Thin Solid Films*, **393**, 40 (2001).
[8] R. Berardi, C. Zannoni. *J. chem. Phys.*, **113**, 5971 (2000).
[9] J. Buey, L. Diez, P. Espinet, H.-S. Kitzerow, J.A. Miguel. *Chem. Mater.*, **8**, 2375 (1996); L. Diez, P. Espinet, J.A. Miguel, M.B. Ros. *J. Mater. Chem.*, **12**, 3694 (2002).
[10] D.J. Mabbot, B.E. Mann, P.M. Maitlis. *J. chem. Soc., Dalton Trans.*, 294 (1977).
[11] P.S. Pregosin, F. Wombacher, A. Albinati, F. Lianza. *J. organomet. Chem.*, **418**, 249 (1991).
[12] A. Bondi. *J. phys. Chem.*, **68**, 441 (1964).
[13] K. Reichenbächer, H.I. Süss, J. Hulliger. *Chem. Soc. Rev.*, **34**, 22 (2005).
[14] K. Praefcke, B. Bilgin, J. Pickardt, M. Borowski. *Chem. Ber.*, **127**, 1543 (1994); B. Bilgin Eran, D. Singer, J. Pickardt, K. Praefcke. *J. organomet. Chem.*, **620**, 249 (2001).

[15] B. Bilgin Eran, C. Tschierske, S. Diele, U. Baumeister. *J. Mater. Chem.*, **16**, 1136 (2006).
[16] J. Buey, P. Espinet. *J. organomet. Chem.*, **507**, 137 (1996).
[17] F. Bisi, E.G. Virga, E.C. Gartland Jr, G. de Matteis, A.M. Sonnet, G.E. Durand. *Phys. Rev. E*, **73**, 051709 (2006).
[18] P.I.C. Teixeira, A.J. Masters, B.M. Mulder. *Mol. Cryst. liq. Cryst.*, **323**, 167 (1998).
[19] M.A. Bates. *Phys. Rev. E*, **74**, 061702 (2006).
[20] M.A. Bates. *Chem. Phys. Lett.*, **437**, 189 (2007).
[21] R. Hooft, B.V. *COLLECT: Data Collection Software Nonius* (1998).
[22] Z. Otwinowski, W. Minor. In *Methods in Enzymology* Vol. 276, C.W. Carter Jr, R.M. Sweet (Eds), pp. pp. 307–326, Academic, New York (1997).
[23] G.M. Sheldrick. *SHELXS-97 and SHELXL-97: Programs for Solution of Crystal Structures*. University of Göttingen, Germany (1997).
[24] R.A. Moore, R. Levine. *J. org. Chem.*, **29**, 1439 (1964); J.P. Anselme. *J. org. Chem.*, **32**, 3716 (1967).